Chapter 8
Gothic Cathedrals

Abstract. Aim of this chapter is the study of statics of Gothic cathedrals, splendid achievements of engineering, and architecture of the Middle Age. Some brief notes give information about times and places of their construction and an introductory analysis describes the structural elements constituting their stone skeleton. Two main static problems are then discussed: evaluation of the wind strength of the whole cathedral structure and analysis of the slender piers instability. The critical wind velocity for the cathedral of Amiens is determined by direct application of the Limit Analysis, via kinematical approach.

The failure occurred at the cathedral of Beauvais in the past 1284 is studied in the second part of the chapter. The failure is generally attributed to the effects of foundations settlements. The chapter, conversely, inquires the possibility that the collapse could be due to piers instability, due to their exceptional height and slenderness. The question is examined in deep, analyzing, in particular, the effects of creep of the mortars on the piers strength. It is shown that the instability of the slender masonry piers, with their axial loadings eccentricities and the mortars creep effects, could be considered really responsible of the 1284 failure.

8.1 Introduction and Historical Notes

During the transition from the Romanesque to the Gothic period many radical changes came about in architectural style, especially in the construction of churches. Gothic cathedrals best highlight the structural originality of the architecture of the time. Large masonry masses were the hallmark of Romanesque constructions and only small windows opened in the perimeter walls of Romanesque churches. In contrast, the construction of a structural skeleton, unrelated to the masonry masses, was the first innovation. Large openings could thus be built into the walls and would eventually give rise to the stained glass and rose windows so typical of Gothic churches.

The main architectural elements of Gothic structures are pointed arches, ribbed cross vaults, flying buttresses, and slender piers, some of which had already been used in Romanesque and, even earlier, in Roman architecture. Simultaneous application of all these elements to form a harmonious, unified whole was first achieved by French architects of *Ile de France,* who redefined the concept of cathedral. A prelude to Gothic architecture can be discerned in the mid-12th-century rebuilding of the apse of the Basilica of Saint-Denis, where French kings were once

M. Como: Statics of Historic Masonry Constructions, SSSSM 1, pp. 465–508.
springerlink.com

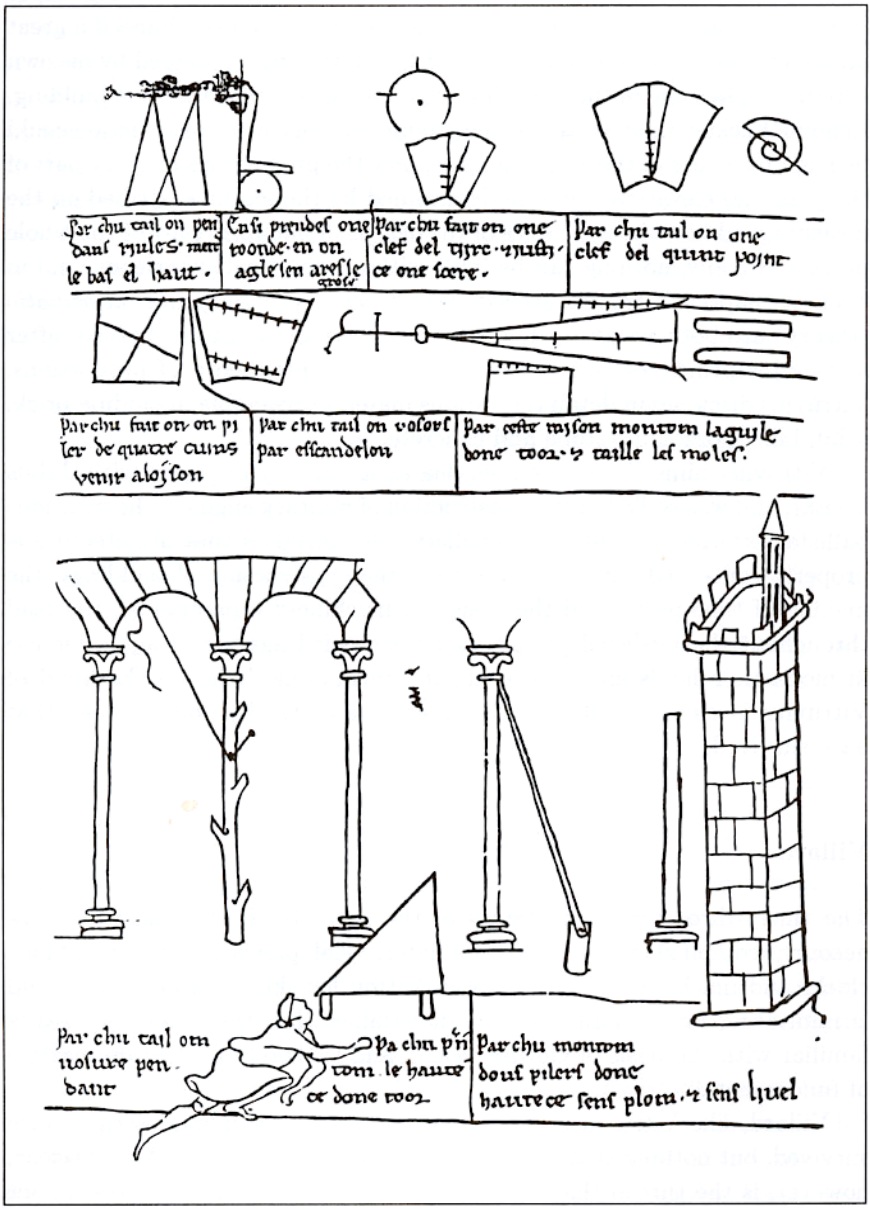

Fig. 8.1. A illustration from the notebook of Villard de Honnecourt (Heyman, 1995)

entombed, under the supervision of Pierre de Montereau and Suger: the broad windows under the arcades of the ogival vaults, supported by slender columns, herald the typical vast interior space of later Gothic cathedrals. Gothic architecture is typified by the cathedrals of Noyon (1160), Notre Dame in Paris (1163), Laon (1170), Saint Remy at Reims (1162 and 1181), and Soissons (1190). Somewhat later, construction of the cathedrals of Chartres (1195–1260) and Amiens (1220–1269), with ribs surrounding the piers starting at their bases and rising to join the vault ribs, gave rise to the Gothic *rayonnant,* which the pioneering naves of Saint Denis had originally introduced. Gradually, Gothic architecture spread throughout Europe and over subsequent centuries cathedrals were built in this magnificent style in nearly every major city.

The "golden age" of cathedral construction began with the inception of the choir of the Basilica of Saint-Denis, in about 1140, and continued up to 1284, the year the Beauvais Cathedral collapsed while still undergoing construction. With the Beauvais design, daring Gothic architecture had reached the extreme limit of static stability.

The principles of mechanics applied by cathedral builders were centered on the use of levers and the composition of forces. Mason lodges jealously treasured their knowledge of these principles, which were passed on during long years of training in workshops and at building sites.

The designers of Gothic cathedrals were at once architects and engineers. The 33 tables, in architect Villard de Honnecourt's notebook, drawn up in about the year 1235, document the techniques used in building sites and for the construction of Gothic cathedrals. Geometry was the sole basis of design: the construction codes, in fact, set out strict rules for proper geometrical proportions (figure 8.1).

8.2 Notes on the Construction Techniques

The stones used by cathedrals builders originated in nearby, frequently marl, quarries. However, marl does not offer high compression strength, so the stones had to be cut precisely to present perfectly flat surfaces and thereby improve contact with the mortar beds. Lime mortars were used. A wall consisted of 2, 20- to 30-cm thick outer layers or facings made of high-quality coursed ashlars, and a rubble and mortar inner filling. The two outer layers were connected by larger through-the-thickness stones in order to connect the two facings at regular intervals. As a rule, foundations were rather undersized: patrons did not enjoy seeing their money 'wasted' on underground structures that no one would ever see. Thus, nearly all the cathedrals built during the period suffered from differential subsidence, but were able to freely follow the settling and maintain an admissible equilibrium. Gothic cathedrals piers are very slender (figure 8.2), though they are well connected to flying buttresses and vaults and, as a rule, well-braced. Buckling is the most common hazard. The aisles of Gothic cathedrals are covered by stone vaults, which are, in turn, covered by wooden trusses. The masonry vaults served to protect the interiors from fire. Figure 8.3 shows the progressive evolution of the transverse sections of three cathedrals built between the years 1190 and 1220: the cathedrals of Soissons, Chartres, andAmiens..

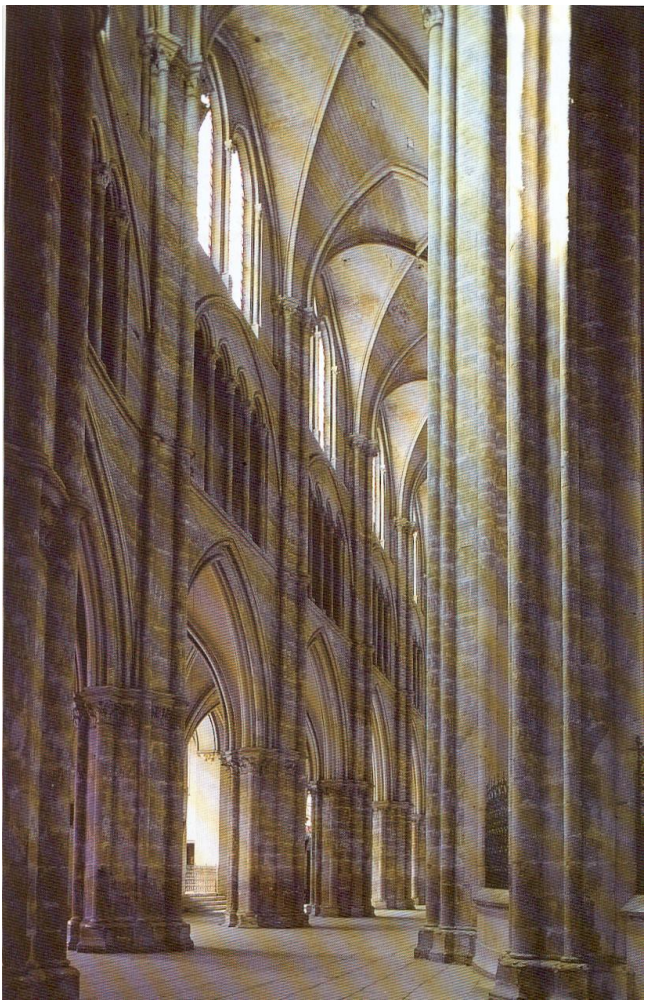

Fig. 8.2. Interior of the Cathedral Saint-Étienne in Bourges

The heights of the extrados of the nave vault increased gradually with improvements in constructional techniques – from 30 meters of the Soissons cathedral and 34 meters at Chartres, up to 42 meters in the Cathedral of Amiens.

The challenge facing Gothic builders was to attain a nave vault height equal to the 48 m of the Beauvais Cathedral, the last cathedral to be built during France's golden age of Gothic architecture.

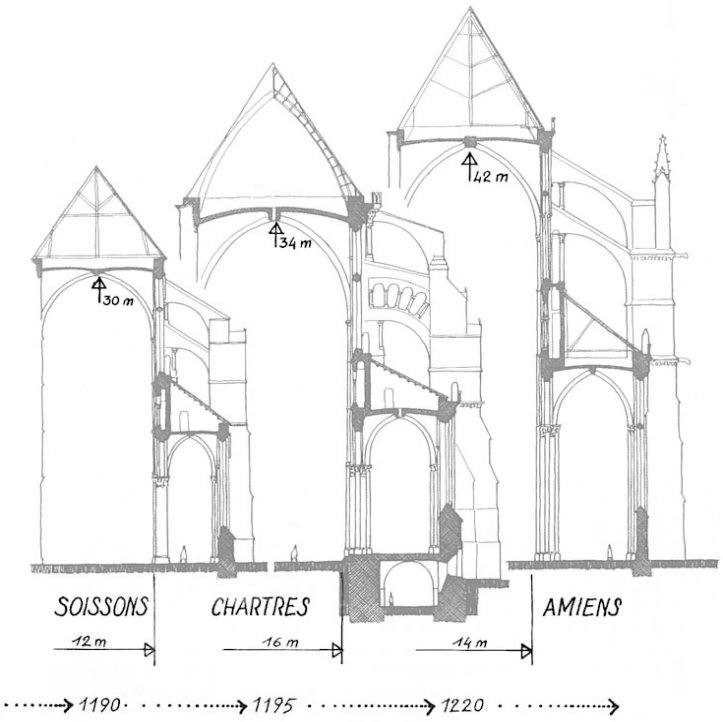

Fig. 8.3. Transverse sections of cathedrals built in successive times: Soissons, Chartres, and Amiens.

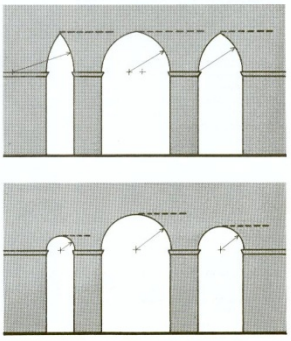

Fig. 8.4. Ogival arches of the same height but different spans. Comparison with rounded arches.

Pointed or ogival, arches were the most commonly used. Pointed arches mark the evolution of vaults spans. Ogival arches offer the advantage of reaching the same height despite the different spans (figure 8.4). A typical cathedral section is

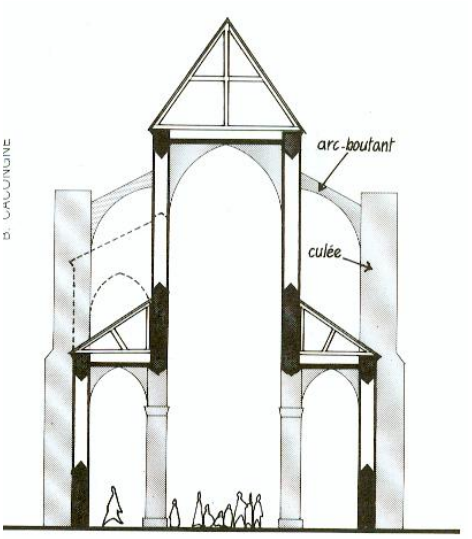

Fig. 8.5. The function of the flying buttress (arc boutant)

illustrated in figure 8.5, where the flying and the external buttress are indicated with their French terms.

The thrust of the nave vault of a major cathedral with lateral aisles is transmitted from above the aisle roofs by the flying buttresses to the external buttresses and thence to the ground. In such cases the flying buttresses work as simple props. The weight of the flying buttress yields a curved pressure line and

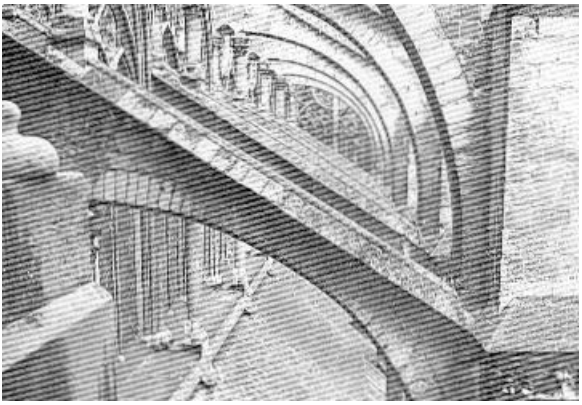

Fig. 8.6. Flying buttresses on the Cathedral of Notre Dame at Amiens

the profile of the flying buttress must thus be that of a flat arch. With its ends fixed it is indeformable and the degree of the bearable thrust is limited only by the masonry crushing strength. Major cathedrals possess a double prop system and so only the lower flying buttresses convey the thrust of the vault. When the cathedral is exposed to the actions of the wind, the upper flyers, which are situated on the windward side, sustain the roof trusses and therefore work just as the lower flyers. The vertical buttresses at the outer end of the flyers were often capped with pinnacles that provide additional vertical loading to help resist the lateral thrust transmitted by the flyer. In the absence of wind, the thrust on the upper flying buttresses is near minimum. Figure 8.6 shows a detail of a flying buttress on the cathedral of Amiens.

8.3 Relevant Static Problems

The landscape of the plains of France is dotted with the distant profiles of cathedrals rising above the more common buildings of many cities and towns. It does not take much imagination to picture the force of the winds blowing through these plains to impinge on the cathedrals' façades and upper structures. Nor is it difficult to understand the enormity of the challenges facing architects of the time in building masonry structures able to oppose the actions of the fierce winds and prevent the buckling of such high piers.

8.4 Transverse Wind Strength

8.4.1 Wind Action

Cathedral structures are rigid in both the longitudinal the transverse directions. Wind action is essentially static and can be represented by a suitable distribution of horizontal forces.

Figure 8.7 shows the typical distributions of wind velocity and pressure acting on the vertical projection of a transverse section of a cathedral. Wind pressure is proportional to the square of the velocity, thus explaining why, while wind velocity increases less than linearly with height, pressure instead increases as a nearly linear function of height.

Air velocity reduces on the windward face, speeds up on the lateral sides, and generates eddies on the leeward side. Wind pressure is thus positive on the windward side, while it is negative on the leeward side, due to the suction produced by the airflow separation.

The reference velocity V_{ref} is generally measured at a height of 10 m from the ground, given that at ground level the velocity falls to near zero. A simple formula, drawn from Canadian building codes, expresses the variation in wind velocity $V(z)$ with height z, relative to the reference velocity V_{ref}:

$$V_{wind}(z_m) = V_{ref}\left(\frac{z}{z_{ref}}\right)^{\alpha}, \tag{1}$$

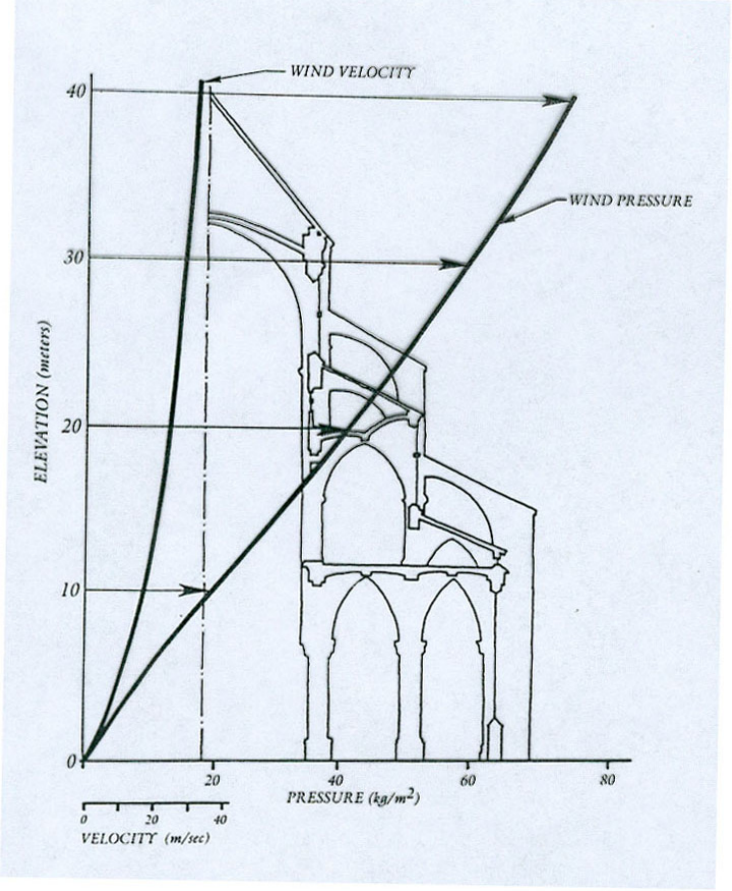

Fig. 8.7. Wind velocity and pressure distributions acting on the transverse section of a cathedral (From Wilipedia)

where, in urban areas, α = 0.35 ~ 0.40. For instance, a wind stream with a velocity of 50 km/h, or 13.9 m/sec, at a height of 10 m from the ground, will at 40 meters' height, have a velocity $(4)^{0.35}$ = 1.62 times larger than V_{ref}, that is, about 24.2 m/sec.

According to the Italian code, the wind pressure on a unit surface orthogonal to the wind direction can be calculated as

$$p_v = q_b c_e c_p, \tag{2}$$

where

$$q_b = 1/2\rho V_b^2, \tag{3}$$

and:

ρ = standard air density taken to be 1,297 kg/m^3;

V_b = wind velocity in m/sec;

c_e= exposure factor, varying with height; this variation can be evaluated via Eq. (1),

c_p= aerodynamic factor, which can be assumed equal to 0.8 on the windward side and - 0.4 on the leeward side.

By way of example, the wind pressure of an air stream with an average velocity of 50 km/h acting over an orthogonal surface on the windward side at a height of 10 m from the ground is

$$p_{v.10m} = \frac{0.5 \cdot 1.297}{9.81} \cdot \frac{\sec^2}{m} \frac{kg_f}{m^3} 13.9^2 \frac{m^2}{\sec^2} \cdot c_e \cdot 0.8 = 10.2 \frac{kg_f}{m^2}.$$

On the leeward side the wind pressure is instead negative and equal to

$$p'_{v,40m} = -5,1 \frac{kg_f}{m^2}.$$

Wind pressure increases greatly with increasing wind velocity: for instance, a 100 km/h wind at 40 m from the ground produces a pressure on the windward side of

$$p_{v,40m} = \frac{0.5 \cdot 1.297}{9.81} \frac{\sec^2}{m} \frac{kg_f}{m^3} (27.77 \cdot 1.62)^2 \frac{m^2}{\sec^2} \cdot 0.8 = 107 \frac{kg_f}{m^2},$$

while on the leeward side it is

$$p'_{v,40m} = -53.5 \frac{kg_f}{m^2}.$$

Wind produces significant actions on cathedral structures, particularly on the piers and buttresses. However, cathedral geometries generally provide adequate strength even for exceptionally strong winds, as will be shown in the following.

Figure 8.8 shows the assumed distribution of the wind pressure acting on the transverse section of a cathedral: here *p and p'* indicate conventional values of the

wind pressure respectively on the windward and leeward sides, and λ is a load multiplier. We assume an approximate wind pressure distribution on the cathedral walls, that is, increasing linearly with the height. The collapse wind pressures $\lambda_{cr}p$ and $\lambda_{cr}p'$ will be obtained via determination of the failure multiplier λ_{cr} by application of Limit Analysis.

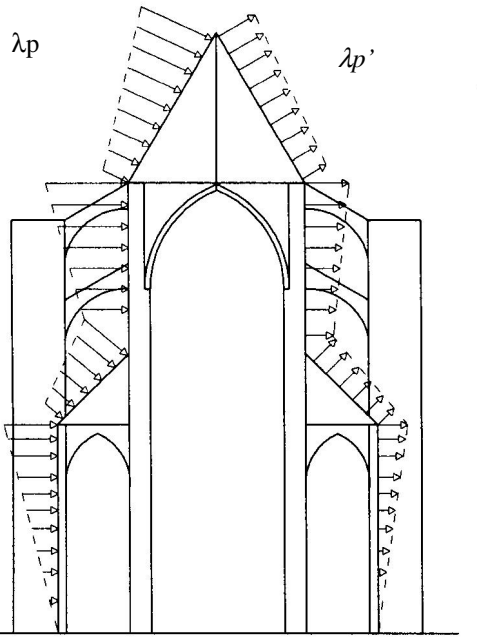

Fig. 8.8. Wind pressure distribution on the transverse section of a cathedral: λp and $\lambda p'$ indicate the wind pressure on the windward and leeward sides

8.4.2 Possible Transverse Failure Mechanisms

Two different failure mechanisms can occur:

a) semi-global, interesting only the leeward side of the cathedral transverse section, as illustrated in figure 8.9 (Sardoni, a.a.2007 – 2008)

b) global, interesting both sides of the cathedral transverse section, as illustrated in figure 8.10. Both the thrust of the vault and the wind pressure on the leeward side contribute to semiglobal failure a), while the wind actions on both the windward and leeward sides combine to bring about global failure b).

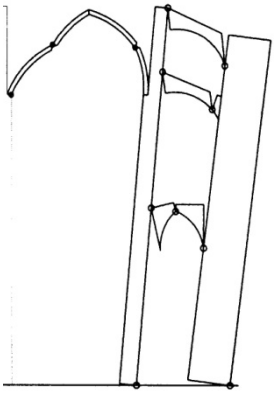

Fig. 8.9. Semiglobal mechanism

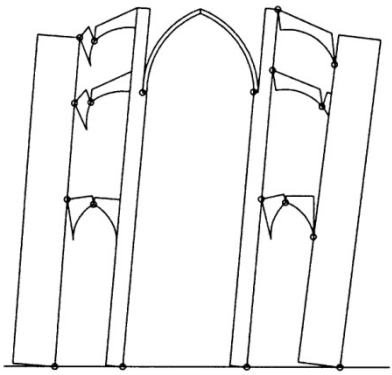

Fig. 8.10. Global mechanism

8.4.3 Cathedral Transverse Modulus

The following analysis considers a cathedral segment with length equal to the longitudinal distance *i* between the piers of the nave.

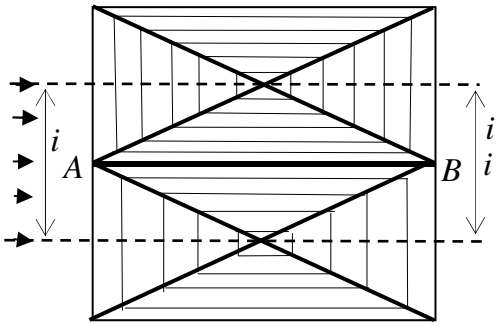

Fig. 8.11. Segment of a cathedral of length *i* equal to the longitudinal span between the piers

The schematic illustrations of a cathedral in figures 8.11 and 8.12 correspond to the segment AB in figure 8.15.

We will follow a kinematic approach to consider the plane problem corresponding to the sectional structure AB of the cathedral. We first define the kinematic geometries of the two mechanisms and then evaluate the work performed by all the forces, dead loads, and wind pressures, acting on the sectional structure, but also taking into account the forces F transmitted by the diagonal ribs of the cross vault to the structural *modulus,* AB, according to the scheme in figure 8.16. Forces F are independent of the wind action due to the presence of longitudinal windowed walls and consist of the vertical load *V* and the minimum thrust *S*.

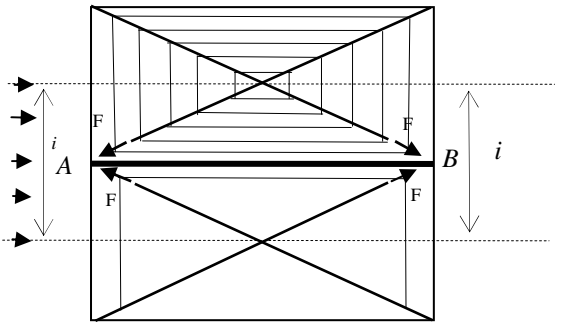

Fig. 8.12. Forces F transmitted by the vault diagonal ribs to the plane structure AB

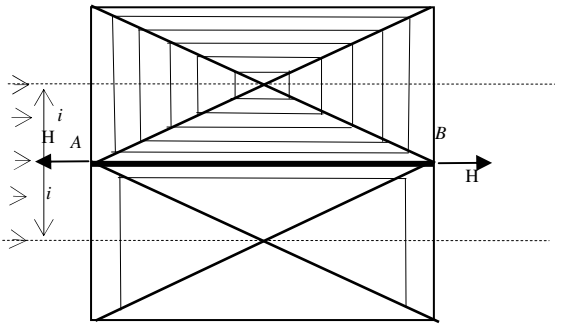

Fig. 8.13. Horizontal thrust H conveyed by the ribs to the flying buttress

8.4.4 Dead Loads Acting on the Various Components of the Structural Modulus

Loads on the Pier

The total height of the pier is H_{1tot}. (fig. 814). The pier is composed of two segments: the first, of length $H_{1,}$ has a circular section of diameter D_1 and is encircled by eight small columns of diameter d. The higher segment of the pier reaches the base of the roof trusses and has length H_{1tot} and a smaller diameter, $d_{2.}$ The total weight of the pier is

$$G_{pier} = (\pi \frac{D_1^2}{4} + 8\pi \frac{d^2}{4}) H_1 \gamma + \pi \frac{d_2^2}{4} H_{1\sup} \gamma .$$

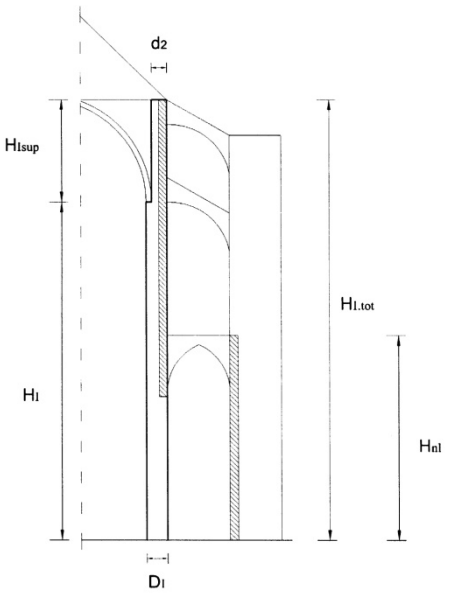

Fig. 8.14. Pier geometry

Weight of the Longitudinal Windowed Wall

The longitudinal wall rises from the extrados of the aisle vaults at H_{n1} up to the springing of the nave vault. The weight of this wall is

$$G_{windowed\ w} = (H_{1tot} - H_{n1}) s \cdot i \cdot \psi_{gl} \cdot \gamma \ ,$$

where s is the full thickness, i is the longitudinal span between the piers, and ψ_{glass} a factor to take into account the glass window surfaces.

Weight of the Longitudinal Arches

These arches run below the windowed wall. Their weight is

$$G_{arches} = H_{arch} s_{arch} \cdot i \cdot \psi_{arch} \cdot \gamma \ ,$$

where H_{arch} indicates the total height of the arch at the springing, s_{arch} the thickness of the arches, and ψ_{arch} a factor to account for the variable height of the arch.

Weight of Half the Transverse Wall at the Cross Vault Extrados

With reference to figure 7.14, we have

$$G_{tr\ \text{wall}} = \frac{L_{nave}}{2} H_{n1} s_w \cdot \psi_w \cdot \gamma \ ,$$

where L_{nave} is the net transverse distance between the piers.

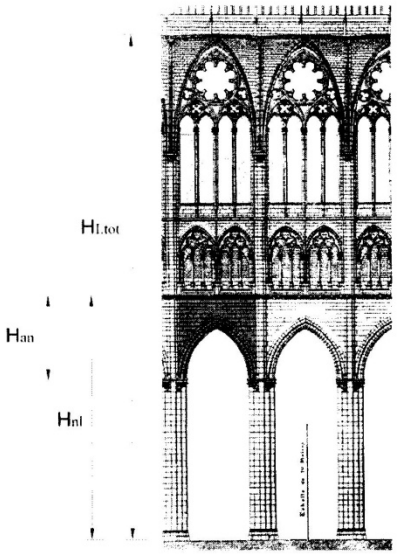

Fig. 8.15. Longitudinal windowed wall with arches

Load Conveyed by the Roof Truss on the Nave and on the Aisle

We assume an average total weight for the roof $q_{roof} = 0.5\text{t/m}^2$, whence we get

$$G_{roof\ n} = \frac{L_{nave}}{2} i \cdot q_{roof} \ .$$

Load Conveyed by the Roof Truss on the Aisle

$$G_{roof\ a} = \frac{L_{aisle}}{2} i \cdot q_{roof} \ ,$$

where L_{aisle} is the net width of the aisle.

Load Conveyed by the Flying Buttresses

A flying buttress has an average height h_{fb}, thickness s_{fb}, *and* diagonal length L_{fb}, hence

$$G_{fb} = s_{fb} \cdot h_{fb} \cdot L_{fb} \cdot \gamma \, .$$

Load conveyed by the nave vault

The minimum thrust transmitted by the ribs is evaluated as shown in figure 7.16.

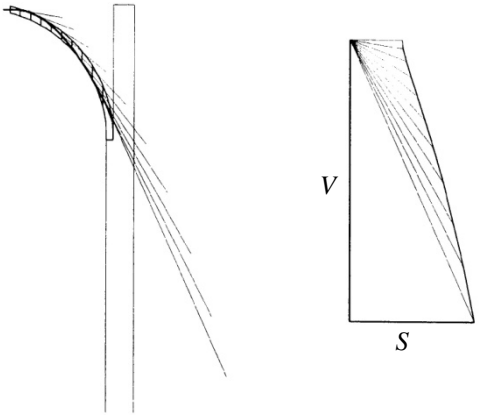

Fig. 8.16. Evaluation of the minimum thrust in the vault ribs

The webs are 30 cm thick and made of brick masonry with a unit weight of 1.6 t/m^3. The ribs are 50 cm thick and made of stone masonry with a unit weight of 1.8 t/m^3. The resultant horizontal thrust transmitted to the flying buttress by the ribs converging at B in figure 7.16 equals 16.5 t, while the vertical action is 41.6t. Load V_{nv} will be obtained in a separate analysis of the vault.

The total load acting on the pier is therefore:

$$G_{tot\ pier} = G_{pier} + G_{windowed\ w} + G_{arches} + G_{tr\ \mathrm{wall}} + G_{roof\ n} + G_{roof\ \mathrm{a}} + G_{fb} + V_{nv}\ .$$

Loads on the buttress

The buttress weight (fig. 7.17) is

$$G_{buttr} = s_{buttr} \cdot H_{buttr} \cdot L_{IV} \cdot \gamma\ .$$

The weight of the external wall is

$$G_{ex\ w} = s_{ex\ w} \cdot H_{ex\ w} \cdot L_{ex\ w} \cdot \gamma\ .$$

Load S_{nv} conveyed by the aisle roof truss

We assume an average total weight of the roof q_{nv} of

$$S_{aisle\ \mathrm{r}} = \frac{L_{II}}{2} \cdot i \cdot q_{\mathrm{nv}}\ .$$

Load S_{nv} conveyed by the aisle vault
Load S_{nv} will be evaluated in a separate analysis of the vault.

Load conveyed by flying buttresses

The flying buttresses have an average height h_{fb}, thickness s_{fb}, *and* diagonal length L_{fb}, hence

$$G_{fb} = s_{fb} \cdot h_{fb} \cdot L_{fb} \cdot \gamma \ .$$

The total load acting on a buttress is therefore

$$G_{tot\ count} = G_{count} + G_{ex\ w} + S_{nv} + S_{aisle\ r} + G_{fb} \ .$$

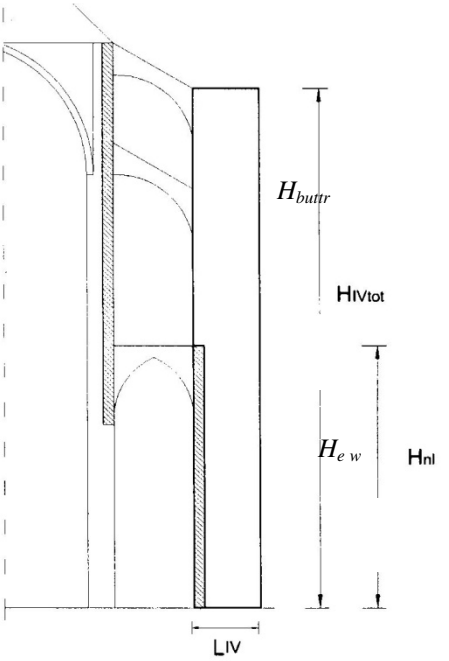

Fig. 8.17. A buttress

.4.5 Lateral Wind Strength of the Amiens Cathedral of Notre Dame

Evaluation of the failure wind distribution in the transverse direction has been performed for the Notre Dame Cathedral in Amiens. Figures 8.18 and 87.19 show the plan and the front view of the cathedral. The cathedral measures about 7,000 m^2 in plan and rises to a height of 43.00 m. The transverse section shows the presence of a double order of flying buttresses. The church has a nave and two lateral aisles, a wide apse, divided into four sectors, and an ambulatory with seven side chapels. Maintaining the previous notation and referring to figures 7.18, 7.19, and 7.20, we have:

Pier:
$H_{tot} = 43.0$ m, $H_1 = 33.0$ m, $D_1 = 1.8$ m, $D_2 = 1.5$ m, d = 0,20 m, $H_{n1} = 20.0$ m,
$G_{pier} = 198$ t,

Longitudinal windowed wall:
$H_{n1} = 20.0$m, $\psi_{glass} = 0.5$, $s = 0.8$ m, $i = 7.5$ m
$G_{windowed\ w} = 124$ t

Longitudinal arches
$H_{arch} = 7.0$ m, $s_{arch} = 0.8$ m, $\psi = 0.5$, $s = 0.8$ m,
$G_{arches} = 38$ t

Half the transverse wall at the cross-vault extrados
$L_{nave} = 12.6$ m, $H_w = 10.0$ m, $s = 0.8$ m, $\psi = 0.5$,
$G_{tr\ w} = 45$ t

Load conveyed by the roof truss on the nave and side aisle
$G_{roof\ n} = 24$ t $G_{roof\ a} = 11$ t

Horizontal thrust H conveyed by the vault to the flying buttress
H = 16.5 t

Vertical load V conveyed by the vault to the pier
$V_{nv} = 41.6$ t

Vertical load V conveyed by the flying buttresses to the pier
$V_{f\ b} = 15$ t

Total load on the pier
$G_{tot\ pier} = 532$ *t*

Loads on the buttress

$s_{butr} = 2.0$ m, $H_{buttr} = 40$ m, $L_{IV} = 5.0$ m, $\gamma = 1600$ kg/m^3
$G_{buttr} = 640$ t

Weight of the external wall
$H_{ex\ w} = 20.0$ m, $s_{ex\ w} = 0.8$ m, $L_{ex\ w} = 5.5$ m,
$G_{ex\ w} = 87$ *t*
Load conveyed by the roof truss on the aisle
$G_{roof\ a} = 11$ t
Load conveyed by the aisle vault
$G_{aisle\ vault} = 20$ t

Load conveyed by flying buttresses
$G_{flying\ b} = 15$ t

Total load on the buttress
$G_{tot\ pier} = 789$ *t*

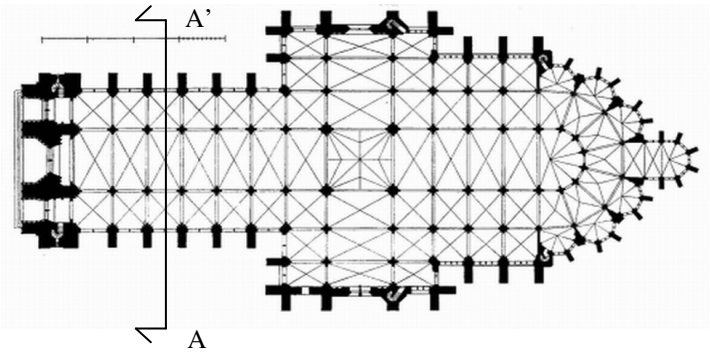

Fig. 8.18. Plan of the Amiens Cathedral

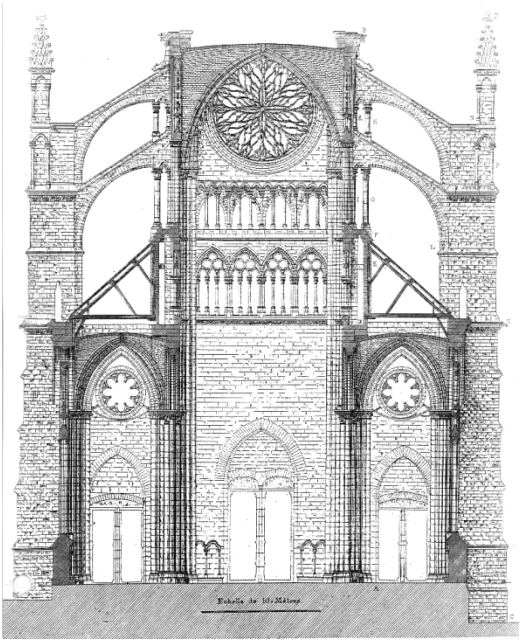

Fig. 8.19. Front view of the Amiens Cathedral

8.4.5 Semi-Global Failure

Semi-global failure occurs with the development of the mechanism shown in figure 8.9. In this case the wind forces act on the leeward side. Figure 8.20 shows the distributions of the wind pressure on the various structural components of the cathedral modulus. The wind pressure varies with the height according to the linear law

$$p_{leew\ w}(z) = \lambda p_o \frac{z}{H} \ ,$$

where λ is the load multiplier and p_o a conventional pressure value assumed to be 150 kg/m^2, and H = 54 m is the height of the top of the trusses on the nave. The pressure acts on the leeward side and produces the following actions, as indicated in figure 87.20:

Action 1) The wind pressure acting on the roof truss at an inclination of 60° relative to the horizontal is thus $p_{roof\ w} = p_w \sin(60°) = 0.86\ p_w$, as shown in figure 8.20.

Action 2) The wind pressure acting on the longitudinal windowed wall from height $H_{cap\ lat}$ = 27m to $H_{1\ tot}$ = 43m.

Action 3) The wind pressure acting on the aisle roof at H_{n1} = 20 m up to height $H_{cap\ lat}$ = 27 m. The roof is inclined 45° with respect to the vertical.

Action 4) The wind pressure acting from the ground up to height H_{n1} = 20 m.

The leeward wind pressure has been taken to be half the windward pressure.

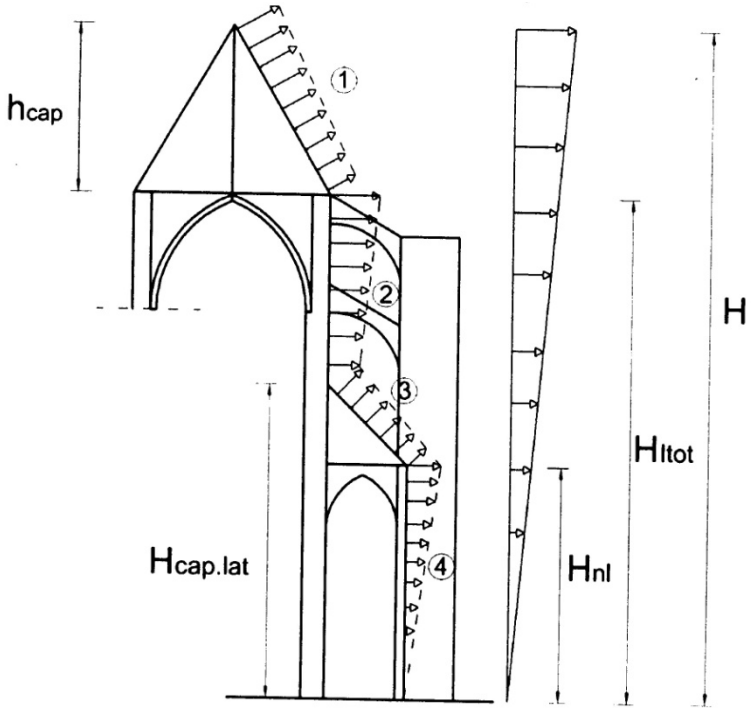

Fig. 8.20. Leeward wind pressure distribution on various cathedral heights

There are actually various different semi-global mechanisms depending on the positions of the hinges (7,8) and (1,7) in the arch defined by the angles,

$$\phi_i\,, \qquad\qquad \phi_e\,,$$

shown in figure 8.21. All the quantities involved are shown in figure 8.21, together with the hinges of the semi-global mechanism. Figure 8.21 illustrates the lateral semi-global mechanism, with the various hinges involved.

The entire leeward side of the sectional modulus of the cathedral moves left. Hinges split the sectional modulus into eight segments, indicated in figure 8.21 as I, II, III,…VII, and VIII. Figure 8.21 instead shows the absolute centers of rotation, (1) and (4), of the pier and buttress, as well as that of the first segment of the arch, (8). Figure 87.21 also indicates the relative centers of rotation as (7,8), (17) ,….etc. The mechanism is completely defined when all the absolute centers of the various segments have been determined.

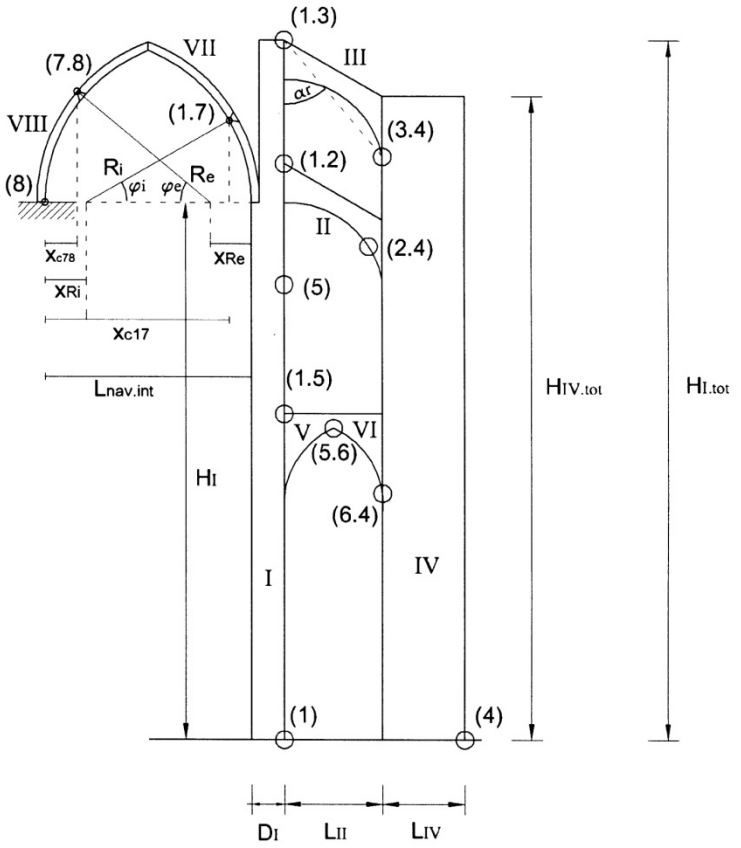

Fig. 8.21. Hinges corresponding to the semi-global mechanism

Let us now determine the positions of these centers, given the alignment conditions between the triplets of the points:

- (8), (7,8) , (7) and (1), (1,7); (7) gives the position of the absolute center (7);
- (1), (1,3), (3) and (4), (3,4); (3) gives the position of the absolute center (3);
- (1), (1,2), (2) and (4), (2,4); (2) gives the position of the absolute center (2).

We must now define the positions of the last centers, (5) and (6). Given that the center positions (1,3) and (3,4) are known, we can evaluate the position of (1,4) by using the alignment condition between the terms (1,3), (3,4), (1,4), and (1), (4). (1,4). We then obtain the position of (2,4) through the alignment condition between the triplets (1,3), (3,4), (1,4), and (1,2), (1,4), (2,4).

We can determine now the position of the relative center (1,6) by taking into account the alignment condition between the terms (1,5), (5,6), (1,6), and (1,6), (6,4), (1,4). Thus, the position of the absolute center (6) follows from the alignment between (1,6), (1), (6), and (6,4), (4), (6). Finally, the alignment between (6), (5,6), (5), and (19, (1,5), (5) furnishes the position of (5) (figure 8.22).

The deformation resulting from the mechanism is defined by the rotation θ_1 of the pier around its absolute center (1), as shown in figure 8.22. All the rotations of the various segments II, III,….VII, and VIII are linearly dependent on rotation θ_1. In order to define these functions it is necessary to evaluate the coordinates of the various centers. Figure 8.23 shows the positions of hinges (1,7), (7,8), and (7).

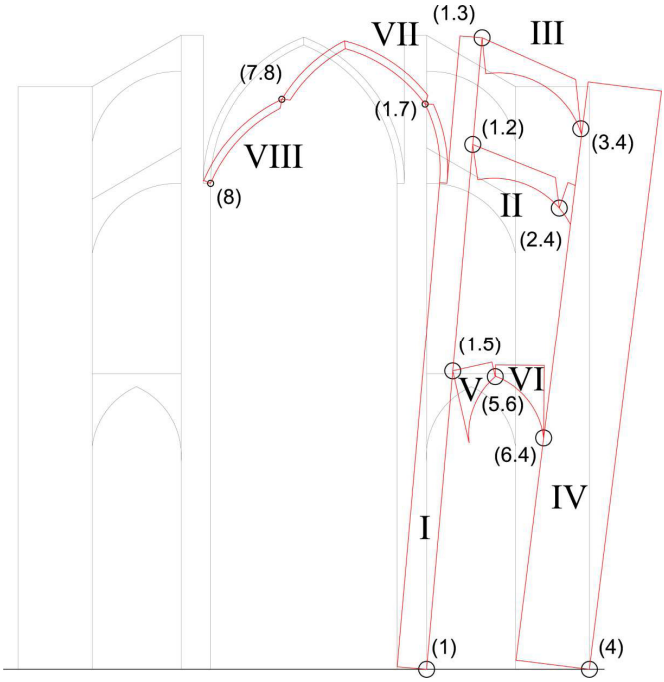

Fig. 8.22. Deformed semi-global mechanism

The pier and the buttress rotate in the clockwise direction. The positions of three of the 12 hinges remain undetermined: hinges (7,8) and (1,7) in the arch, and hinge (2,4) in the lower flying buttress.

The positions of the relative hinges (7,8) and (1,7) depend on the angles ϕ_e and ϕ_i:

$$x_{(7,8)} = L_{nave} - [R_e \cos(\phi_e) + x_{\mathrm{Re}}] \qquad y_{(7,8)} = R_e \sin(\phi_e)$$

$$x_{(1,7)} = R_i \cos(\phi_i) + x_{\mathrm{R}\,i} \qquad y_{(1,7)} = R_i \sin(\phi_i)$$

Evaluating the position of absolute center (7) requires knowing the angles η and β defined in figure 8.23. To this end, we have

$$\eta(\phi_e) = arctg \frac{y_{(7,8)}(\phi_e)}{x_{(7,8)}(\phi_e)} \qquad \beta(\phi_i) = arctg \frac{y_{(1,7)}(\phi_i)+H_I}{L_{nave}-x_{(1,7)}(\phi_i)+D_I}.$$

Quantity $x_{t,}$ defined in figure 8.23, is

$$x_t = \frac{y_{(1,7)}}{tg\beta}$$

and

$$x_7 = \frac{\frac{tg(\beta)}{tg(\eta)}[x_{(1,7)}+x_i]}{1+\frac{tg(\beta)}{tg(\eta)}} \qquad y_7 = tg(\eta)\frac{\frac{tg(\beta)}{tg(\eta)}[x_{(1,7)}+x_i]}{1+\frac{tg(\beta)}{tg(\eta)}}.$$

We can now obtain the expressions for the absolute rotations θ_{VII}, θ_{VIII}, θ_{IV} which depend linearly on the rotation θ_I of the pier (fig. 8.24 and 8.25):

$$\theta_{VII} = \theta_I \frac{(L_{nave}-x_{(1,7)}+D_I)}{x_{(1,7)}-x_{(7)}} \qquad \theta_{VIII} = \theta_{VII} \frac{(x_{(7)}-x_{(7,8)})}{x_{(7,8)}}$$

$$x_{(1)-(1,4)} = H_{Itot} \cdot tg(\alpha_r) \qquad x_{(4)-(1,4)} = x_{(1)-(1,4)} - (L_{II} + L_{IV})$$

$$\theta_{IV} = \theta_I \frac{x_{(1)-(1,4)}}{x_{(4)-(1,4)}}.$$

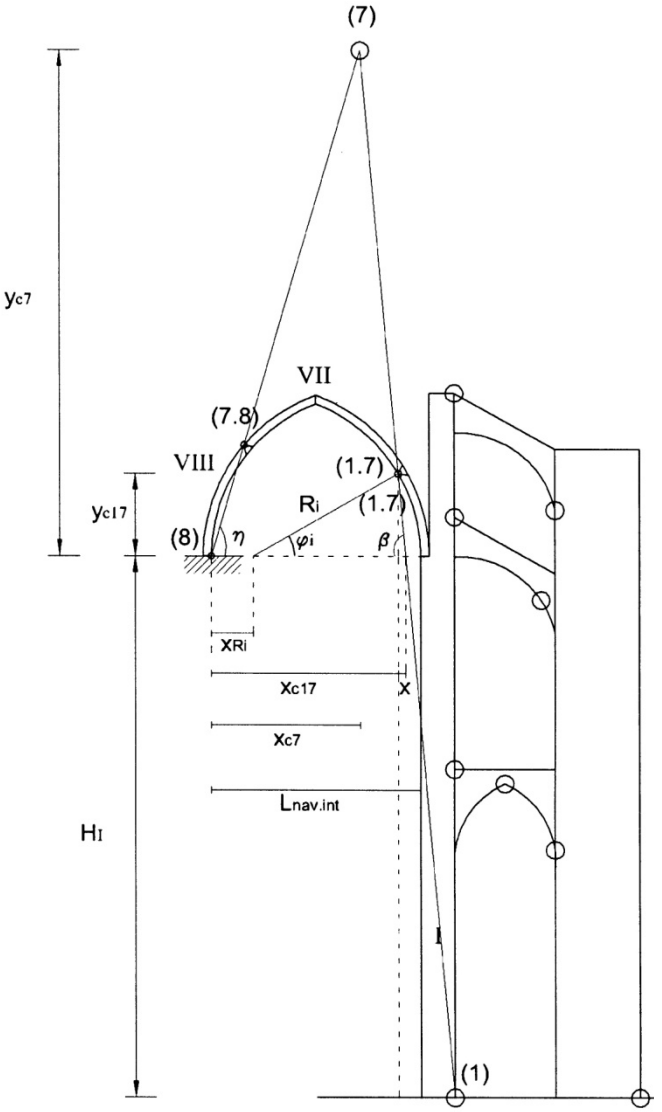

Fig. 8.23. The various distances defining the centers of rotation of the semi-global mechanism

The work performed by the loads acting on the flying buttresses and the aisle vault are negligible with respect to the work of the loads on the pier and the buttress. We can therefore consider only the rotations θ_I , θ_{VII}, θ_{VIII} , θ_{IV} .

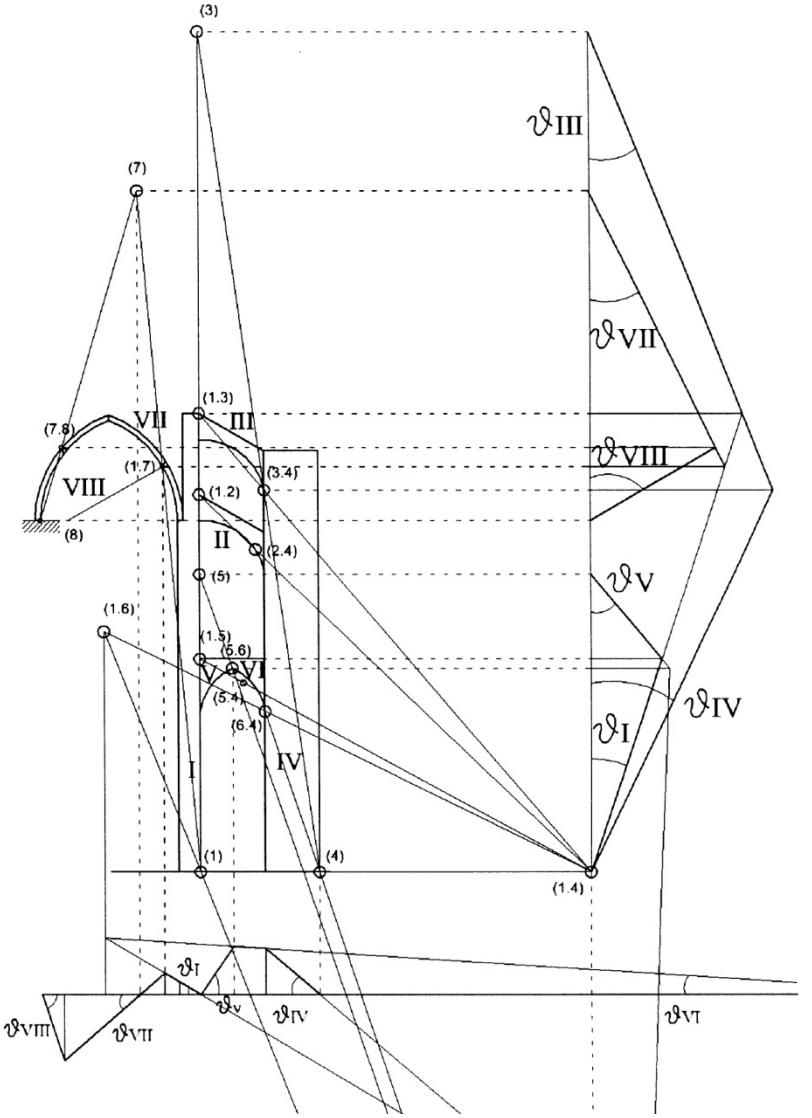

Fig. 8.24. Overall semi-global mechanism with all the centers of rotation and vertical/horizontal displacements

During development of the mechanism the dead and wind loads, modified by multiplier λ, perform the work <g,v> and λ<p_w, v>. The equilibrium condition

$$< g, v(\phi_i, \phi_e) > + \lambda < p_w, v(\phi_i, \phi_e) >= 0 \qquad (4)$$

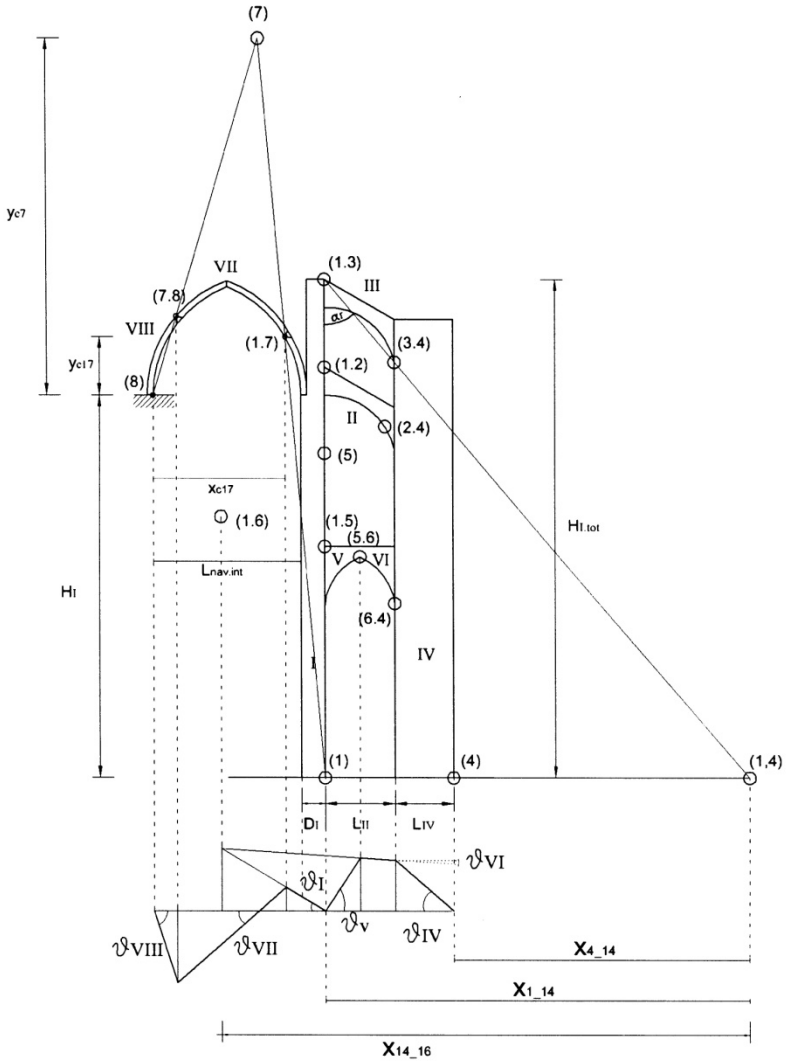

Fig. 8.25. Positions of the centers of rotation of the semi-global mechanism

furnishes the kinematic multiplier

$$\lambda(\phi_i, \phi_e) = -\frac{<g, v(\phi_i, \phi_e)>}{<p_w, v(\phi_i, \phi_e)>}. \tag{5}$$

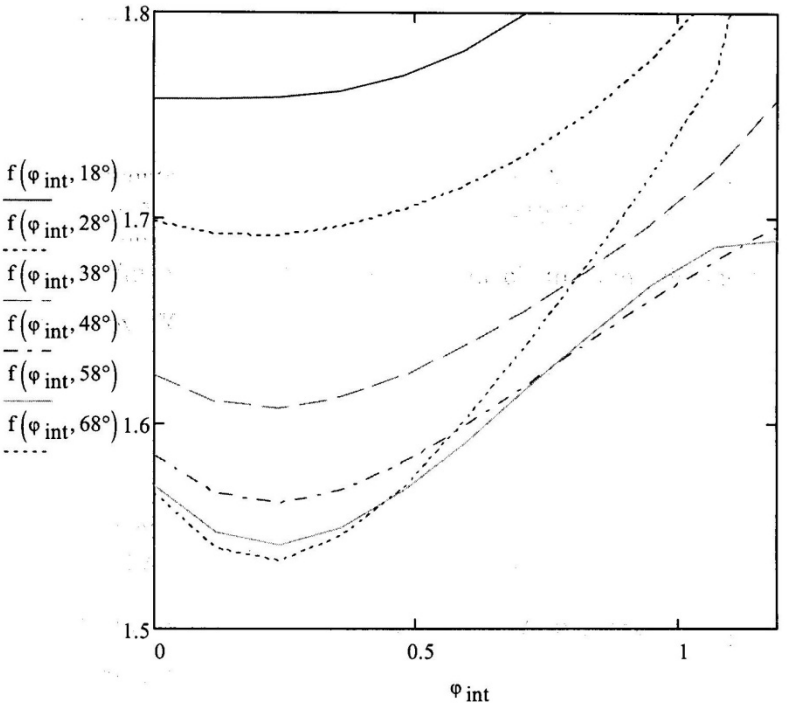

Fig. 8.26. Variation of kinematic multiplier $\lambda(\phi_i, \phi_e)$ with varying angles ϕ_i and ϕ_e. The minimum of $\lambda(\phi_i, \phi_e)$ is attained at ϕ_e = 68° and ϕ_i 12.269° (0.214 rad)

The minimum of λ can be sought for by varying the two parameters, ϕ_e, ϕ_I , defining the positions of hinges (7,8), (1,7):

$$\lambda_{cr} = \underset{\phi_i,\phi_e}{Min} \left[-\frac{<g, v(\phi_i,\phi_e)>}{<p_w, v(\phi_i,\phi_e)>} \right] . \tag{6}$$

The analysis has been conducted assuming a conventional wind pressure value on the windward side of 150 kg/m^2. The program MathCAD has been utilized to determine the minimum of the kinematic multipliers λ by evaluating work $<g, v(\phi_i, \phi_e)>$ and $<p_w, v(\phi_i, \phi_e)>$, taking into account the vertical and horizontal displacements of the various segments, as shown in figure 8.24. Both the expressions for the rotation angles and the different wind pressure values on the leeward and windward sides have been considered. The obtained minimum value λ_{cr} is (Orsini S., a.a. 2011 – 2012)

$$\lambda_{cr}(\phi_i, \phi_e) = 1.533 . \tag{7}$$

The corresponding collapse pressure of the wind acting on the windward side is

$$p_{coll} = \lambda_{cr}(\phi_i, \phi_e)\, p_o = 1.533 \cdot 150 = 230 \text{ kg/m}^2$$

and the critical wind velocity at a height of 57 m turns out to be

$$V_{cr\ H=57m}\sqrt{\frac{2 \cdot 230 \cdot 9.81}{1.3 \cdot 0.4}} = 93m / \sec \ . \tag{8}$$

The corresponding wind velocity at 10 m height is thus given by the condition

$$93m / \sec = V_{cr\ H=10m}\left(\frac{57}{10}\right)^{0.4} ,$$

which yields $V_{cr\ H\ =\ 10\ m}$ = 46.3 m/sec = 167 km/h. The values of angles ϕ_e, ϕ_I that minimize $\lambda(\phi_e, \phi_I)$ are respectively

$$\phi_e = 1.187 \text{ rad } (68°) \qquad \phi_I = 0.214 \text{ rad } (12°,27) \tag{9}$$

as shown in figure 8.26 and 8.27.

Consequently, the positions of hinges (7,8) and (1,7) are determined as:

$x_{(7,8)}$ = 6.11 m $y_{(7,8)}$ = 6.11 m
$x_{(1,78)}$ = 12.37 m $y_{(1,7)}$ = 2.14 m .

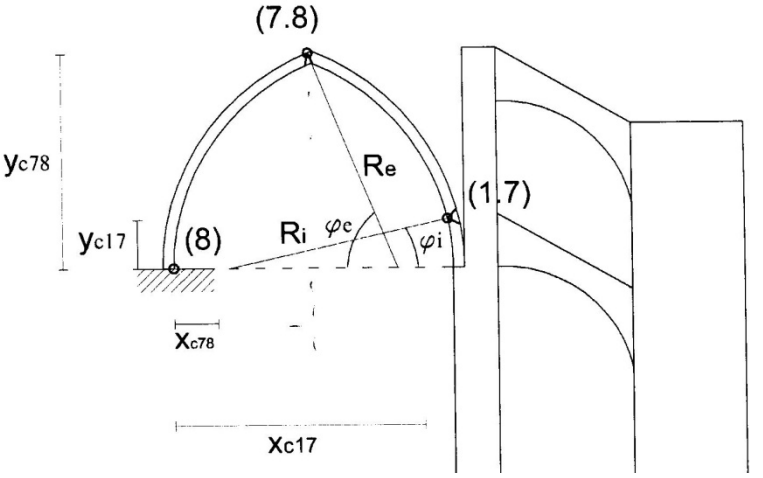

Fig. 8.27. Positions of internal hinges in the arch in critical state

8.4.6 *Global Collapse Mechanism*

The global mechanism is illustrated in figure 8.28 a. Let us first consider only the leeward side of the sectional modulus of the cathedral.

Hinges split the sectional modulus into 11 segments, indicated in figure 8.28 as I, II, ,…X, and XI. Figure 8.26 shows the absolute centers of rotation (1) and (4) of the pier and the buttress. Figure 8.28 b also indicates the relative centers of rotation as (1,2), (1,3) ,….etc. The vault on the nave does not deform because the trusses connected to the pier top sections require that the horizontal displacements between these sections *be equal*. We thus have

$$u_A = u_B \tag{9}$$

whence

$$\theta_{VII} = \theta_I \,. \tag{9'}$$

Let us now go on to evaluate the positions of the absolute centers of rotation. The following alignment condition between the turns of the rotation points hold:

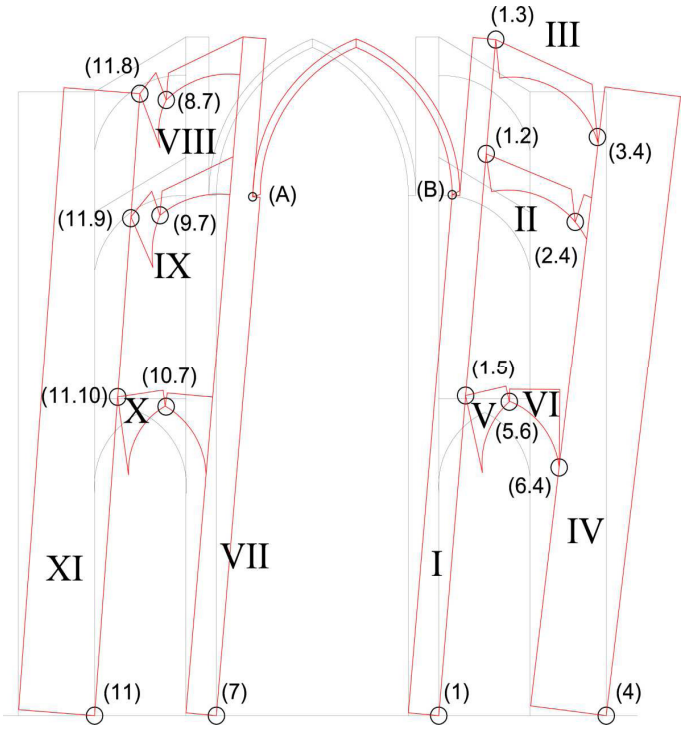

Fig. 8.28 a. Overall deformed global mechanism of the leeward side of the cathedral modulus

The alignment conditions between the triplets of the points:

(1,3), (3,4), (1,4) - (1), (4), (1,4) gives the position of relative center (1,4);
(1), (1,2), (2) - (4), (2,4), and (2) gives the position of absolute center (2);
(4), (3,4), (3) - (1), (1,3), and (3) gives the position of absolute center (3);
(1,4), (6,4), (1,6) - (1,6), 1,5), (5,6) gives the position of relative center (1,6);
(1,4), (5,6), (4,5) - (1,4), (4,5), (1,5) gives the position of relative center (4,5);
(4), (4,5), (5) - (1), (1,5), and (5) gives the position of absolute center (5);
(1), (1,6), (6) - (5), (5,6), (6) gives the position of absolute center (6).

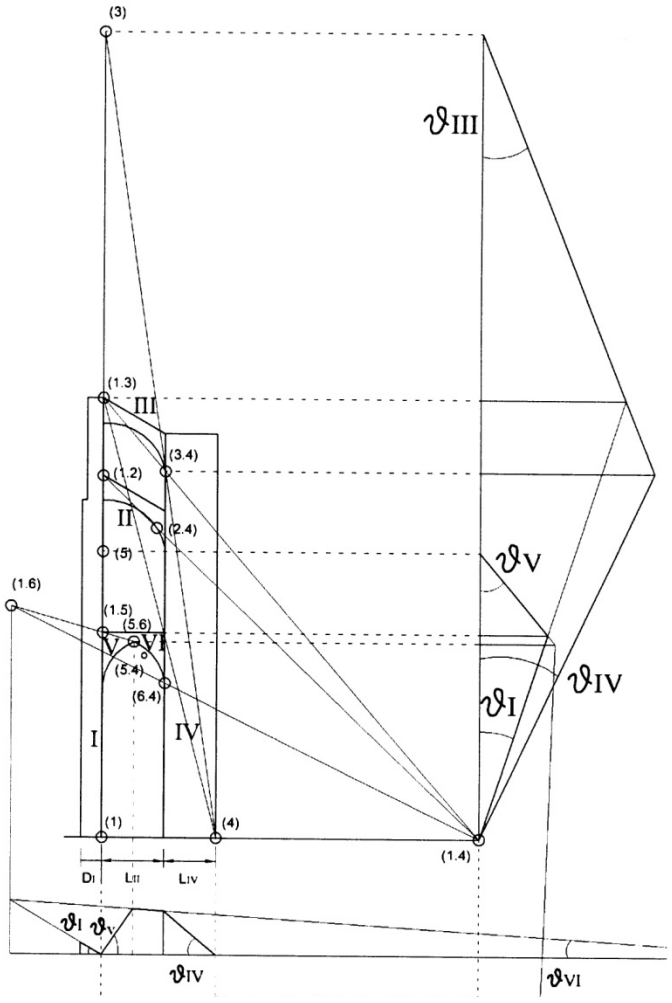

Fig. 8.28 b. Overall global mechanism involving the leeward side of the cathedral modulus with the corresponding centers and displacements

Relative center (1,4) belongs to both pier I and buttress IV. The pier rotates around (1) by angle θ_I and the buttress by angle θ_{IV} around (4). Figure 8.28 b indicates the distance $x_{(1)-(1,4)}$ between centers (1) and (1,4), whence we have

$$x_{(1)-(1,4)}\theta_I = x_{(4)-(1,4)}\theta_{IV} \ .$$

The distance $x_{(1)-(1,4)}$ can be easily expressed in terms of the tangent of angle α_R between the line connecting (1,3) and (3,4) with the vertical. Thus, we have

$$tg\alpha_R = \frac{x_{(1)-(1,4)}}{H_{Itot}} \ .$$

At the same time

$$x_{(4)-(1,4)} = x_{(1)-(1,4)} - (L_{II} + L_{IV}) \ ,$$

whence we obtain the rotation of buttress IV:

$$\theta_{IV} = \frac{x_{(1)-(1,4)}}{x_{(4)-(1,4)}}\theta_I \ .$$

Likewise for the other rotation angles θ_{VI} and θ_V, we have

$$\theta_{VI} = \frac{x_{(1)-(1,6)}}{x_{(1)-(6)} + x_{(1)-(1,6)}}\theta_I \qquad \theta_V = \frac{L_{II}\theta_{VI} + 2L_{IV}\theta_{IV}}{x_{(1)-(6)} + x_{(1)-(1,6)}} \ .$$

The work performed during development of the mechanism by the dead loads acting on the flying buttresses and on the aisle is minor and can be neglected. We can thus dispense by evaluating the rotations θ_{II} and θ_{III}.

Let us now consider the windward side of the cathedral modulus. The left buttress is now indicated as segment XI and the pier as segment VII. The two fliers are respectively segments VIII and IX and the vault on the aisle is segment X.

The relative centers of rotation (11,8), (11,9), and (11,10) are localized at the extrados of the sections connecting fliers VIII and IX and vault X (figure 8.28 c). The figure also shows the absolute centers of rotation (11) and (7) of the buttress and the pier. Center (10,7) is located at the intrados of the central section of the vault spanning the aisle. We must now evaluate all the positions of the remaining absolute and relative centers of rotation. Analogously to the foregoing, the following alignment condition hold between the triplets:

(11), (11,10), (10), and (1), (10,7), (7) gives the position of absolute center (10);

(7,11), (11,8),(7,8), and (8),(7,8), and (7) gives the position of relative center (7,8);

(74), (9,7), (9), and (11), (11,9), and (9) gives the position of absolute center (9);

(11), (11,8), (8), and (8), (8,7), (7) gives the position of absolute center (8).

We can now define angle α_P between the line connecting the centers (11,10) and (10,7) with the vertical as :

$$tg\alpha_P = \frac{L_{nl}/2}{H_{(11,10)} - H_{(10,7)}} \ ,$$

and the distance between centers (11) and (7,11) is given by

$$tg\alpha_P = \frac{x_{(11)-(7,11)}}{H_{(11,10)}} \ .$$

We can now evaluate the values of the absolute rotations of the various segments.

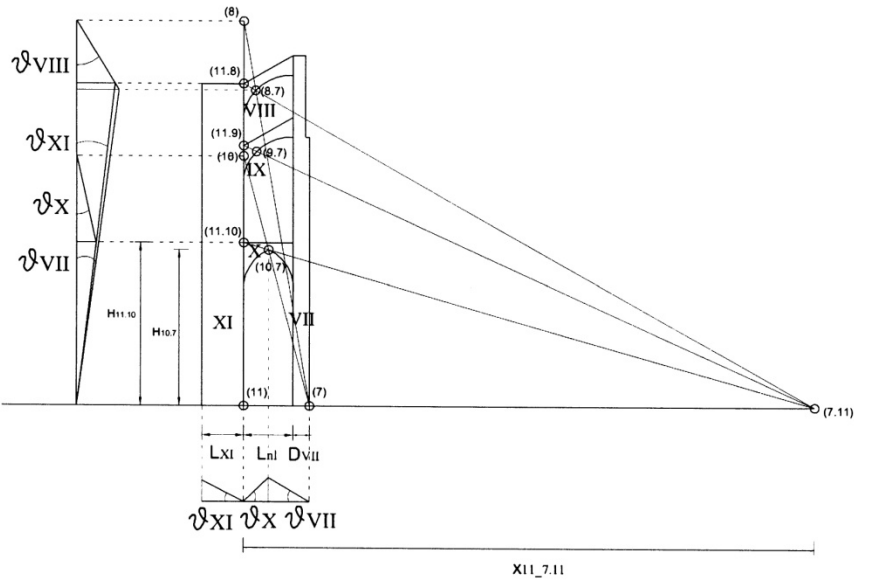

Fig. 8.28 c. Positions of the various centers of rotation and displacements occurring on the windward side in the global mechanism

Relative center (7,11) belongs to both pier VII and buttress XI. The pier rotates around (7) by angle θ_{VII} and the buttress by angle θ_{XI} around (11). Figure 8.27 indicates the distance $x_{(11)-(7,,11)}$ between centers (11) and (7,11). We thus have

$$x_{(11)-(7,11)}\theta_{XI} = [x_{(11)-(7,11)} - (L_{nl} + D_{VII})]\theta_{VII}$$

and obtain the rotation of the buttress as a function of rotation of the pier:

$$\theta_{XI} = \frac{[x_{(11)-(7,11)} - (L_{nl}+D_{VII})]}{x_{(11)-(7,11)}}\theta_{VII} \ .$$

Likewise, we also obtain:

$$\theta_X = \frac{L_{nl}+2D_{VII}}{L_{nl}}\theta_{VII} \ .$$

During development of the mechanism the dead and wind loads, modified by multiplier λ, perform the work $<g,v_{gl}>$ and $\lambda<p_w, v_{gl}>$, where v_{gl} indicates the global mechanism. The equilibrium condition

$$< g, v_{gl} > + \lambda < p_w, v_{gl} >= 0 \tag{10}$$

thus furnishes the failure multiplier corresponding to the global mechanism

$$\lambda_{cr\ gl} = -\frac{<g,v_{gl}>}{<p_w,v_{gl}>} . \tag{11}$$

Using the *MathCAD* program, the critical multiplier has been evaluated as (Orsini S., a.a. 2011 – 2012)

$$\lambda_{cr\ gl} = 1.116 . \tag{12}$$

The windward pressure is

$$p_{cr\ gl} = 1.116 \cdot 150 = 167.4\ kh/m^2 \ , \tag{13}$$

and the corresponding critical wind velocity at a height of 57 m takes the value

$$V_{cr\ H=57m}\sqrt{\frac{2 \cdot 167.4 \cdot 9.81}{1.3 \cdot 0.4}} = 79.5 m/\sec \ . \tag{14}$$

The corresponding wind velocity at 10 m height can thus be determined via the condition

$$79.5m / \sec = V_{cr\ H=10m}(\frac{54}{10})^{0.4}$$

which furnishes $V_{cr\,H\,=\,10\,m}$ = 40,5 m/sec = 146 km/h. (Orsini S., a.a. 2011 – 2012)

8.4.7 Conclusions

Transverse failure of the model of the Amiens Cathedral comes about through a global mechanism. Evaluation of the corresponding critical wind velocity at a height of 10.0 m from the soil yields the value $V_{cr\,H\,=\,10\,m}$ 146 km/h.

8.5 Creep Buckling Conjecture on the Failure of the Beauvais Cathedral

8.5.1 Introductory Notes

In many respects, the *Cathédrale Saint-Pierre de Beauvais* may be considered the most daring achievement of Gothic architecture; it is made up solely of a transept and choir apse with seven apse-chapels. The vaulting in the interior exceeds 48 m in height, to make it the tallest cathedral in Europe.

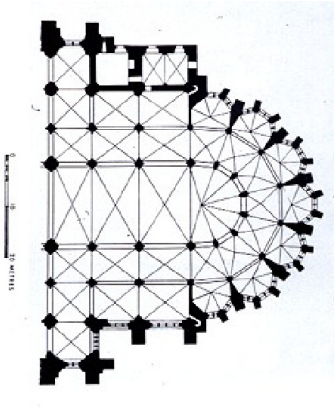

Original plan of the choir and apse

Fig. 8.29.a.

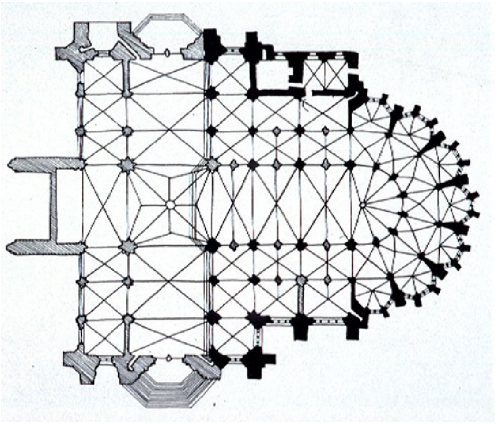

Plan with transept

Fig. 8.29.b.

Construction of the choir and apse was begun in 1247 and finished in 1272. The work was interrupted in 1284 by the collapse of the choir vaulting. The work of reconstructing it spanned the following 50 years and included the addition of extra

piers between the original ones of the choir, so that the bays were halved from about 9 m to 4.5 m in breadth (fig. 8.29 a and 8.29 b). It was in fact thought that the original pier spacing of the failed choir was too large. The choir was completely rebuilt by about 1337, but the work was interrupted for the next 150 years due to the 100 Years War. It was not until 1500 that work on the transept was taken up again and brought to completion in 1548. In 1573, the collapse of the extremely high central tower halted the work once again. Various attempts were made to complete the cathedral, but by 1605 the decision was taken to consolidate the existing structure and abandon the enterprise, leaving it incomplete. Beauvais became what it is today, a choir and transept without a nave. A detailed history of the building has been provided by Branner (1962).

The 1284 failure was quite inexplicable: the cathedral had stood in good condition for 12 years and there are no historical accounts of earthquakes or wind storms occurring before the collapse. Figure 8.30 shows Benouville's (1891–1892) reconstruction of the state of Beauvais in the years 1272–1284 (fig. 8.30).

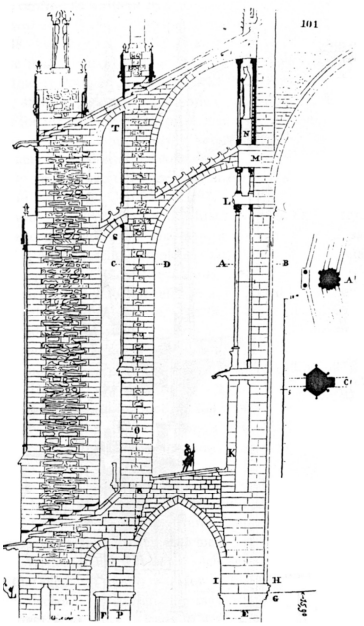

Benouville's reconstruction

Fig. 8.30.

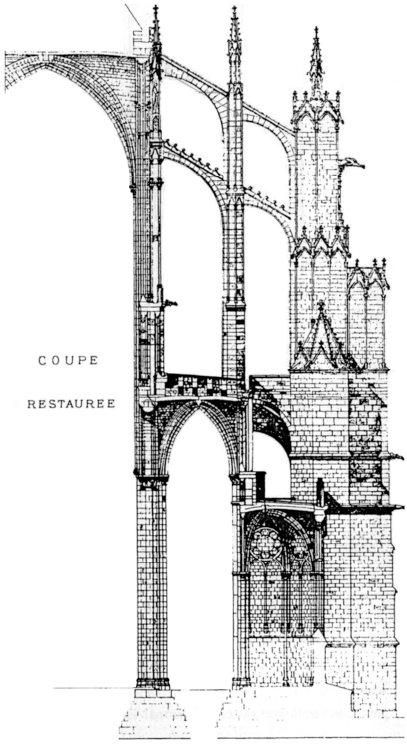

Cross-section at the "*chevet*" (Viollet-le-Duc)

Fig. 8.31.

Figure 8.31 shows the details of the piers at the *chevet*, as illustrated by Viollet le Duc. The cause of the 1284 collapse has long been a matter of a great deal of speculation. Some *slow action* seems to be the most likely cause.

Two different conjectures on the identity of these slow-moving actions have been advanced: creep of the pier mortar and uneven foundation subsidence.

According to Viollet-le-Duc (1858–1868), the mortar creep triggered the transfer of loads from the masonry piers to the adjacent slender marble columns illustrated in figure 8.31. As a consequence, the columns buckled, producing rotation of the so-called *tas de charge,* and consequent distortion of the adjacent flying buttresses with failure of the central vaults and piers.

Heyman (1995), instead, considered it more likely that uneven subsidence of piers foundations, due to soil consolidation, were responsible for the catastrophic collapse. Wolfe and Mark (1976) challenged this conjecture. Firstly, they noticed that there are no signs of any major differential subsidence in the existing building. Moreover, the cathedral was probably built on the site of a preexisting building, near the walls of an old Roman precinct.

Determining for certain the cause of the fall of the original vaults of Beauvais cathedral is naturally a difficult, if not impossible, task, especially given that any and all documentary evidence on the failed construction has been long lost. Nevertheless, some insight into the issue can be gained from the following considerations. First of all, it should be noted that, while the distance between the centers of the main piers was 15 m – the same as many other cathedrals, such as Amiens, Chartres, etc. – the Beauvais piers were considerably higher. Moreover, the piers' cross-sections were much smaller and the means by which they were stiffened, represented by the adjacent slender marble columns, seems very doubtful. It appears that no one ever performed a scientific analysis of the piers' buckling under the loads of the original quadripartite vaults, except perhaps a rather simplistic, conservative evaluation through application of Euler's elastic theory, as recently reported by Mark and Wolfe (1976). In this regard, however, in preceding sections we have seen the dramatic effects of load eccentricities on the buckling strength of masonry piers, whose behavior is very different from Eulerian columns.

Figures 8.30 and 8.31 show the complex geometry of the piers of the Beauvais cathedral, with all their offsets and misalignments, which produce eccentricities in the axial loads. In addition, we have also seen how mortar creep slowly increases the destabilizing effects of eccentric axial loads. Accordingly, it seems natural to harbor strong suspicions that the piers' slenderness, combined with their geometrical irregularities and mortar creep, could have been responsible for the failure.

The next sections will delve more thoroughly into this hypothesis. However, to this end, it is first necessary to obtain a preliminary estimate of the order of magnitude of all the forces acting on the cathedral piers.

8.5.2 Thrust of the Cross Vault Spanning the Choir

With the aim of evaluating the various actions transmitted by the vault to the piers, the following provides a brief static analysis of both the cross vault spanning the choir and transept and the two adjacent flying buttresses (fig. 8.32).

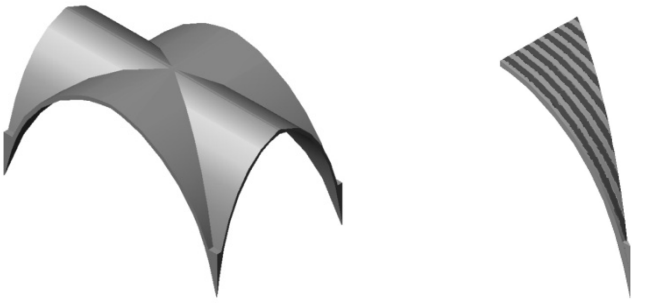

Fig. 8.32. The cross vault spanning the transept The sliced web

The cross vault rib is loaded by its weight and the vertical and horizontal forces conveyed by the sliced arches dividing the webs, each of which is assumed to have a thickness of 25 cm and made of strong bricks. The small inflexions of the vertical buttresses yield minimum thrust states in the sliced arches and cross ribs of the vault. The thrust has been evaluated by Magrì and Iannotti (2004-2005), who also took in account the presence of filling near the vault corners (fig. 8.33).

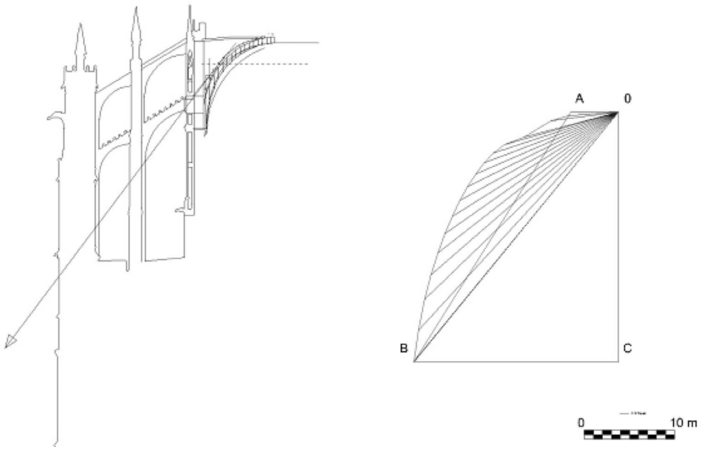

8

Fig. 8.33. Minimum thrust conveyed by diagonal cross ribs on a pier

The thrust of the cross vault ribs is transmitted to the flying buttress across the *tas de charge,* the large marble block that joins the cross vault ribs and the lower flying buttress, as shown in figures 8.33 and 8.34.

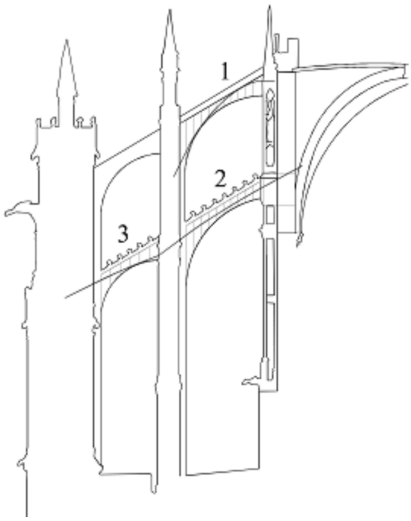

Fig. 8.34. Lines of thrust of the lower and upper flying buttresses

According to calculations, the vertical and horizontal components V and H of force S transmitted by the vault to the pier are about 58 and 19 t, respectively (fig.8.24). The lower flying buttress intercepts this force S on the internal edge of the pier and transfers it through an intermediate pier to the large vertical buttress. The lines of thrust of the lower and upper flying buttresses have been traced. The thrusts of the higher and the lower fliers are respectively near the minimum and maximum thrust values. The lower flier effectively acts as a compressed prop.

8.5.3 Loads Acting on the Piers

The pier has a height of about 44.80 m, as measured from the foundation level to the extrados of the *tas de charge*. The pier is fixed here because of the presence of the flier, on the inner side, and the springing of the nave cross vault, on the other (fig.8.35).

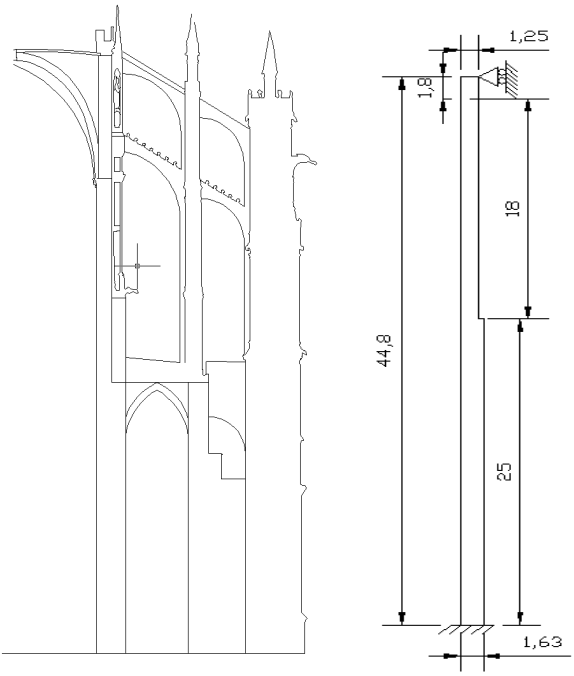

Fig. 8.35. Section of the Cathedral at the transept and two parts of the pier. Lengths in *m*

Above the *tas de charge* the pier extends for about another 7 m to become part of the upper transverse walls. The total length of the pier is thus about 44.80 + 7.00 = 51.80 m, of which 3.80 m run from the foundation to the floor level.

The length of the pier under examination can be subdivided in two main parts (fig. 8.35). The lower, 25 m-long section, extends from the foundation level to the extrados of the side vault, with its first 3.80 m built into the foundation; its circular cross-section is about 1.60 m in diameter. The second part, of 18 m length, is misaligned with respect to the first and reaches the extrados of the *tas de charge*. This section of the pier length, which is approximately circular in cross-section with a diameter of 1.25 m, is strengthened by four adjacent small, slender marble columns with circular cross-sections, each about 0.15 m in diameter. The center of these four columns is at a distance of about 0.625 + 0.35/2 = 0.80 m from the axis of the adjacent pier's cross-section (fig. 8.26).

The lower flier takes the horizontal component of force *S* transmitted by the main vault, so only vertical loads act on the pier. In particular, these latter forces acting on the pier section located just at the vault springing are due to:

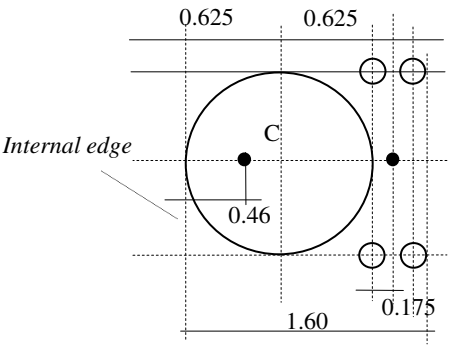

Fig. 8.36. Section of the upper pier with the four small columns. (Lengths in *m*)

1) weight of the roof and the wooden trusses:
Considering an average weight of 500 kg/m^2 in plan, we have:
$W_{roof} = 9.00 \cdot 7.60 \cdot 0.5 = 34.2\ t$, applied along the masonry pier axis, at a distance of 1.25 *m*/2 = 0.625 m from its internal edge (i.e. the edge towards the nave).

2) weight of the transverse masonry walls:
Considering an average area of $8.50 \cdot 9.00\ m^2$, a thickness of 0.5 *m*, a reduction factor of 0.65, to take into account the presence of the openings, a specific gravity of 2 tons/m^3, we have, including the pier weight:

$$W_{sup.wall} = 9.00 \cdot 8.50 \cdot 0.5 \cdot 0.65 \cdot 2 = 49.4\ t$$

This force is also applied along the pier axis, i.e., at a distance of 0.625m from its internal edge.

3) weight of the marble statue on the extrados of the *tas de charge*:
We have approximately: $W_{statue} = 4\ t$, which force acts along the axis of the four small circular columns cross-sections at a distance $e = 0.625 + 0.35/2 = 0.80\ m$ from the center of the pier cross-section.

4) weight of the solid masonry block atop the marble columns, between the external edge of the pier and the upper flying buttress:

$$W = 0.80 \text{ x } 1.05 \text{ x } 1.80 \text{ x } 2.2 = 3.3 \text{ t}$$

5) weight of the pinnacle:

$$W = \pi \cdot 1.0^2/(3 \cdot 4) \cdot 3.0 \cdot 2.2 = 1.7\ t.$$

Both of these last forces act along the axis of the four marble columns, situated at a distance of about $d = 0.625 + 0.35/2 = 0.80\ m$ from the center of the pier section.

6) vertical actions conveyed by both the cross vault spanning the transept and the lower flying buttress.

In a minimum thrust state the vault conveys a vertical force of *58 t,* while the vertical counterthrust of the lower flying buttress is 8 t. Consequently,

$$W_{vault,fl.buttr} = 58 - 8 = 50\ t\ .$$

This force acts along the *internal edge* of the upper pier and thus at a distance of – 0.625 m from the center of the pier cross-section.

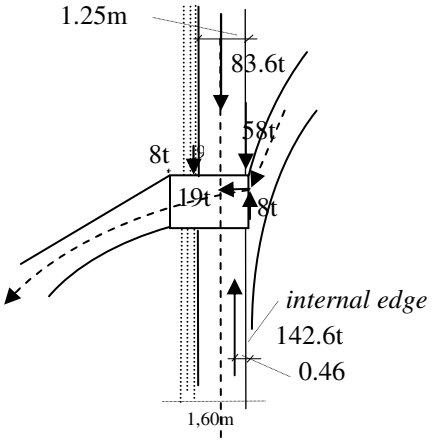

Fig. 8.37. All the forces transmitted across the *tas de charge*

The resultant

Summing up all the above forces:

$$W_{tot} = 83.6 + 4 + 3.3 + 1.7 + 50 = 142.6\ t.$$

By evaluating the moment of all these forces around the center of the pier section, we obtain the eccentricity of the resultant force:

$$83.6 \cdot 0 + 4 \cdot 0.80 + 3.3 \cdot 0.80 + 1.7 \cdot 0.80 - 50 \cdot 0.625 = 142.6\xi,$$

whence $\xi = -0.17\ m$.

The distance of W_{tot} from the internal edge of the pier at the extrados of *the tas de charge* is $e = 0.625 - 0.17 = 0.46\ m$

The center of the composite section made up of the sections of the pier and four columns is very near the center of the pier's section itself. The core of this composite section is about 15 cm in width. Consequently, the two external marble columns, placed on the outer side, would have to be *unloaded*. The eccentric axial load is for all intents and purposes sustained solely by the circular masonry cross-section of the pier head.

Finally, at its springing the side vault spanning the aisle transmits to pier the following vertical and horizontal actions:

$$V_2 = 21\ \text{t} \qquad H_2 = 4.8\ \text{t}\ .$$

These forces are applied at the external edge of the pier section at its intersection with the side vault.

8.5.4 Creep Buckling of the Piers

A stability analysis of the pier has been conducted by applying the delayed modulus approach, according the results shown at Sect. 7.2.6.

The complex geometry of the Beauvais piers (fig.8.38) has been inputed into the program Athena (Cervenka et al. 2002) in 2D form. (Di Carlo, 2005-2006) The uppermost length of the pier, the marble stone of the *tas de charge*, exhibits the greatest strength, in both compression and tension.

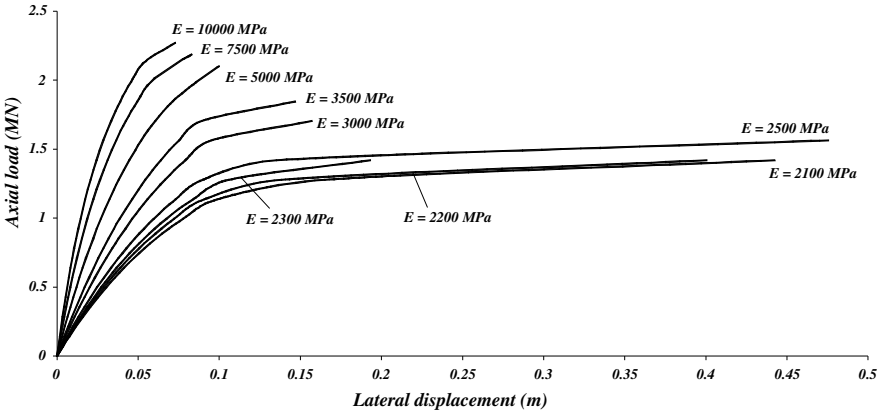

Fig. 8.38. Axial load – lateral displacement curves for different values of the delayed elastic modulus for the Beauvais pier

Because of the eccentricity of the axial load, the small slender marble columns adjacent to the masonry pier have not been taken into account. The pier is loaded at its top section by an axial load P = 142 *t,* with eccentricity e = 0.46 m, as well as other loads applied along its length. The program automatically includes the weight of the various pier lengths.

All the loads are corrected via the parameter λ, which varies in the interval (0, 1), so that all the loads are effective when λ reaches unity. The horizontal displacement Δ of the pier is evaluated at the level of the side vault extrados, where the pier section changes dimensions.

The various axial load versus lateral displacement curves have been plotted by gradually increasing λ for different values of the delayed elastic modulus (fig.8.38).

Due to the long-term creep effects in old mortars, the delayed modulus can also be assumed to be four times lower than the initial value of *E*. Taking into account the order of magnitude of the initial pier masonry elastic modulus, whose value ranges from 10000 to 5000 Mpa, and the corresponding decay due to creep effects, the pier clearly results to be quite unstable.

It is in fact worth noting that when the modulus is near its initial value, the pier exhibits rather good axial strength and would fail only under loads much larger than the actual ones. For delayed modulus values that take into account the strong creep effect, on the other hand, the pier is prone to delay failure under its ordinary loads. Figures 8.39 and 8.40 provide a representation of the different inflexions of the pier under the action of the full loads by gradually reducing the values of the delayed elastic masonry modulus (Di Carlo, 2005-2006).

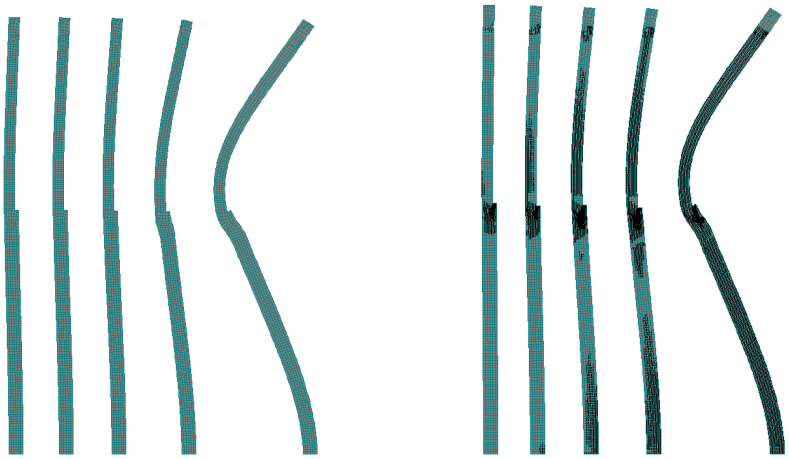

Fig. 8.39. Pier deformations corresponding to modulus values of 10000, 7500, 5000, 2100 MPA - Cracks distribution by gradually increasing load parameter λ in the case of E = 2100 MPa

8.5.5 Conclusions

The structural failure that struck the Beauvais Cathedral in 1284 can in all likelihood be attributed to the slenderness of its masonry piers, with their axis misalignments and eccentric loading, compounded by the inevitable effects of mortar creep. The loads on the lower length of the choir piers are highly eccentric due to the section change occurring at the extrados of the side vaults.

The pier is subject to lateral inflexion, which is exacerbated by the destabilizing effects of the axial loads due to their eccentricity and axis misalignments. The lower part of the pier bends and moves slowly toward the nave. Such displacement cannot be constrained by the side vault, which, as it bears a mechanism deformation and is in a minimum thrust state, follows the lateral inflexion of the pier. The upper part of the pier, fixed at the top by the presence of the fliers and the main cross vault, undergoes strong counter-flexing.

Despite all these deformations and the destabilizing effect of the axial loads, the pier equilibrium would turn out to be stable, if only its initial elastic no-tension response were considered. However, creep deformations of the medieval mortars has gradually aggravated both the pier inflexion and the destabilizing action of the

axial loads. Thus, the pier slowly moved through ever more precarious equilibrium states up to the disastrous failure.

All told, these results allow for concluding that the 1284 collapse of the Beauvais Cathedral was likely due, in part, to delayed creep instability of the masonry piers.

References

Abruzzese, D., Como, M., Lanni, G.: On the horizontal strength of the masonry Cathedrals, Rapp. Sc. del Dipart. di Ingegneria Civile, vol. (29). Univ. Di Roma Tor Vergata (1990)

Benouville, L.: Etude sur la Cathédrale de Beauvais. Encyclopédie d'Architecture, S. 4,4, Paris, pp. 52–54, 60–62, 68–70 (1891-1892)

Branner, R.: Le Maitre de la Cathédrale de Beauvais Art de France, Paris, vol. 2, pp. 77–92 (1962)

Cervenka, V., Cervenka, J.: Atena Program documentation. User's manual for Atena 2D, Prague (June 2002)

Choisy, A.: Histoire del l'Architecture, Paris (1899)

Como, M.: Principi costruttivi e tecniche esecutive delle cattedrali gotiche. In: Morabito, G.(a cura di) (ed.) Europa: Civiltà del Costruire: Dodici lezioni di Cultura Tecnologica Dell'architettura. Gangemi editore, Roma (2004)

Frankl, P.: Gothic Architecture, London, p. 101 (1962)

Heyman, J.: Beauvais Cathedral. Transactions of the Newcomen Society 40, 15–36 (1967-1968), London (1971)

Heyman, J.: The Stone Skeleton. Cambridge University Press (1995)

Jessop, E.L., Shrive, N.G., England, G.L.: Elastic and Creep Properties of Masonry. In: Proceedings of the North American Masonry Conference, pp. 12.1–12.17. The masonry Society (1978)

Morabito, G.: Caratteri e tecniche del costruire nell'Europa del Medioevo. In: Morabito, G. (a cura di) (ed.) Europa: Civiltà del costruire: dodici lezioni di cultura tecnologica dell'architettura. Gangemi editore, Roma (2004)

Shrive, N.G., England, G.L.: Elastic, creep and shrinkage behavior of masonry. Intern. Journ. of Masonry Construction 1(3) (1981)

Viollet–le–Duc, E.E.: Dictionnaire raisonné de l'architecture francaise du XI^{e} au XVI^{e} Siècle, Paris, 10 vols. (1858-1868)

Wolfe, M.I., Mark, R.: The collapse of the vaults of Beauvais Cathedral in 1284. Speculum 51(3) (1976)

Wolfe, M.I., Mark, R.: The collapse of the vaults of the Beauvais Cathedral in 1284. Speculum 51(3), 462–476 (1976)

Yokel, F.Y.: Stability and load capacity of members with no tensile strength. Journ. of the Struct. Div. ASCE 27(ST7) (1971)

Theses (University of Rome Tor Vergata, Fac. of Engineering)

Di Carlo, F.: Verifica della stabilità dei pilastri non resistenti a trazione sotto carico di punta eccentrico: un'applicazione ai pilastri della cattedrale di Beauvais (2005-2006)

Magrì, G.: Analisi delle volte a crociera della cattedrale di Beauvais, supervisor Como, M. (2004-2005)

Sardoni, S.: La resistenza della cattedrale gotica all'azione del vento, supervisor, Como, M. (2007-2008)
Orsini, S.: Resistenza al vento delle cattedrali, supervisors Como, M., Coccia, S. (2011-2012)

Como, M.: Exercises in the Course in "Statics of masonry historic constructions", Faculty of Engineering, Un. of Roma Tor Vergata, Rome (Italy)
Pavone, A.: Calcolo della spinta della volta a crociera della cattedrale di Beauvais (1994)
Iannotti, A.: Approfondimenti sul Calcolo della spinta della volta a crociera della cattedrale di Beauvais (1995)